ELSEVIER

Comput. Methods Appl. Mech. Engrg. 169 (1999) 311–330

Computer methods in applied mechanics and engineering

Characterization of electromagnetic devices via reduced-order models

J. Eric Bracken, Din-Kow Sun, Zoltan Cendes*

Ansoft Corporation, Four Station Square, Suite 660, Pittsburgh, PA 15219-1119, USA

Abstract

Efficient procedures are presented for simultaneously characterizing the time and frequency domain behavior of 3D electromagnetic devices. The procedures work in the complex-frequency domain on either the finite element or boundary element formulation of Maxwell's equations. Various approximation techniques are used to derive reduced-order models describing the system transfer functions of the 3D device. Two different methods for evaluating reduced-order models are presented. One is called Asymptotic Waveform Evaluation (AWE) and is combined with the finite element method; the other is called Adaptive Lanzcos–Padé Sweep (ALPS) and is combined with the boundary element method. The resulting reduced-order models provide the frequency domain behavior of the device over a broad bandwidth. Using the inverse Laplace transform, these reduced-order models can also provide the time domain behavior of the device. Several numerical examples have been run using commercial EDA software to demonstrate that this solution procedure is a highly efficient and accurate way to characterize the electromagnetic performance of real-life devices. © 1999 Elsevier Science S.A. All rights reserved.

1. Introduction

Time-domain and frequency domain procedures are often used to characterize passive linear electromagnetic devices. In a time-domain method, such as the FDTD or TLM algorithms [1], Maxwell's equations are discretized in both space and time, and time-stepping is used to compute the temporal evolution of the field throughout the solution region. In a frequency-domain method, such as the usual finite element and boundary element methods, Maxwell's equations are written in terms of s or $\dot{\omega}$ and the fields in the solution region are computed at a set frequency. In either case, problems must be solved over and over again to determine the transient response to a variety of different excitations, or to find the frequency response over a broad bandwidth.

This paper presents a different approach. We develop procedures to compute a reduced-order model of the transfer function of the passive linear electromagnetic system. This reduced-order model is derived in the complex frequency domain. Since the response of an initially relaxed linear system is determined by its transfer function, both the time-domain and frequency domain response of the system can be computed from the reduced-order transfer function without the need for additional field solutions.

The transfer function of a linear system described by ordinary differential equations may be expressed as a rational polynomial in terms of its poles and zeros. For a system described by partial differential equations, such as Maxwell's equations, the number of poles and zeros is infinite. Thus, to be computational tractable, we need to approximate this infinite set by computing only the dominant poles and zeros of the system. The resulting approximation to the transfer function is called a reduced-order model. Two different procedures exist in the literature for finding reduced-order models of large linear systems. One is called Asymptotic Waveform Evaluation (AWE) [2–5] and the other is called the Padé Via Lanczos (PVL) algorithm [6]. Both of these procedures were originally applied to the solution of electronic circuits; here we extend these procedures to make them suitable for electromagnetic analysis.

* Corresponding author. Tel: +1 412 261 3200; Fax: +1 412 471 9427; E-mail: zol@ansoft.com

0045-7825/99/$ – see front matter © 1999 Elsevier Science S.A. All rights reserved.
PII: S0045-7825(98)00160-1

There are several advantages to the s-domain approach. First, the electromagnetic transfer function is computed only once. Since the system is linear, there is no need to compute electromagnetic fields over and over again by stepping either through time or frequency. Second, s-domain solutions are fast. Once the electromagnetic transfer function is computed, frequency sweeps and transient analyses take only seconds or even fractions of a second. Third, the electromagnetic analysis may be performed by using either differential or integral equation methods. In this paper, we employ both the finite element method and the boundary element method to compute the transfer function. Fourth, s-domain solutions may be converted into equivalent electrical circuits. These equivalent circuits can be combined with external voltage and current sources and the entire system modeled by using circuit simulators. And fifth, it is very easy to use these reduced-order models in 'what-if' system-level designs. Since the electromagnetic characterization is done once and for all, it is possible to pass very compact yet detailed models on to design groups working at the system level.

Early work on s-domain methods in electromagnetics was performed by Newman [7] and by Kottapalli et al. [8]. An AWE-based fast sweep method for integral equations was first presented in 1992 [9]. The first fast-sweep method that combined asymptotic waveform evaluation with the finite element method was presented in 1993 [10]. An improved form of the PVL algorithm called ALPS for use with integral equations was presented in 1996 [11]. AWE has been employed in the finite element based electromagnetics simulation package HFSS to provide a fast frequency sweep capability since 1993 [12]. ALPS has been employed in the boundary element based electromagnetics simulation package Maxwell Strata since 1996 [13].

This paper begins by introducing the two main approaches to s-domain analysis: Asymptotic Waveform Evaluation (AWE) and Padé Via Lanczos (PVL). We also develop improvements to these methods called Complex Frequency Hopping (CFH) and Adaptive Lanczos–Padé Sweep (ALPS). We then derive reduced-order models from the differential form of Maxwell's equations combining Asymptotic Waveform Evaluation with the finite element method. This is followed by the generation of reduced-order models from the integral form of Maxwell's equations, combining Adaptive Lanczos–Padé Sweep with the boundary element method. Finally, we develop procedures for obtaining transient results from reduced-order models. These transient results are obtained by creating circuit equivalents for the reduced-order models and computing the transient response via standard circuit simulators. The procedures are illustrated with several examples from practical microwave circuit design.

2. Asymptotic Waveform Evaluation (AWE)

AWE begins by applying the Laplace transform to the linearized time-dependent Maxwell's equations. This converts Maxwell's equations into a form dependent on the complex frequency parameter s. Using the Laplace transform and numerical discretization, both the differential form or the integral form of Maxwell's equations can be written in the form.

$$A(s)x(s) = b(s)\,. \tag{1}$$

Here, $x(s)$ is a vector consisting of the desired solution quantities, i.e. electric and magnetic fields with differential methods, current densities and charges with integral methods, $b(s)$ is a vector containing the contributions of applied sources, and $A(s)$ is the matrix generated by the discretization.

The impulse response of this linear system is defined as

$$H(s) = [A(s)]^{-1} bu(s) \tag{2}$$

where $u(s)$ is the Laplace transform of the unit impulse (Dirac delta) function and b is a constant column vector. For a finite-order system like a lumped circuit, this impulse response is a rational function

$$H(s) = \frac{\beta_0 + \beta_1 s + \beta_2 s^2 + \cdots + \beta_q s^q}{\alpha_0 + \alpha_1 s + \alpha_2 s^2 + \cdots + \alpha_q s^q} \tag{3}$$

A rational $H(s)$ may also be written in the factored form

$$H(s) = \frac{b_{q-1}(s - z_{q-1})(s - z_{q-2}) \cdots (s - z_1)}{a_q(s - p_q)(s - p_{q-1}) \cdots (s - p_1)} \tag{4}$$

where the p_i and the z_i are the poles and zeros of the system, respectively.

We may therefore represent any component of the solution vector x_i by using a low-order rational function that is a good approximation over a certain frequency band to the exact (high-order) one. A well-known procedure for accomplishing this task is the Padé approximation [14]. The first $2q + 1$ terms of the Taylor series expansion for (2) about the point s_0 are computed (see [2,3,5] for details) and matched to the Taylor coefficients of the reduced-order model. This results in the equation

$$H(s) = \sum_{n=0}^{2q} (s - s_0)^n \cdot xh_n = \frac{\beta_q(s - s_0)^q + \cdots + \beta_1(s - s_0) + \beta_0}{\alpha_q(s - s_0)^q + \cdots + \alpha_1(s - s_0) + \alpha_0} \tag{5}$$

This can be solved by cross-multiplying the denominator of the rational function and then equating terms with like powers of $(s - s_0)$. An approximation accurate over a broad frequency band can often be determined by computing just 10 to 20 terms of the Taylor series expansion. Once we have a formula characterized in terms of just a few parameters and a_i and b_i, it is a simple matter to evaluate the frequency response by substituting in a particular value of s.

A measure of the quality of the Padé approximation is provided by the matrix residual

$$\text{Error}(s) = \frac{\|A(s)x(s) - b(s)\|}{\|b(s)\|} \tag{6}$$

where $A(s)$ and $b(s)$ are the same as in (1). Computing this matrix residual in a finite element problem is very efficient, because the matrix vector multiplication involves the coefficient matrix which is very sparse. Even in a boundary element solver the residual computation consumes far less CPU time than is required for matrix decomposition, and it provides a good indicator of the accuracy of the solution. A large matrix residual indicates a poor solution. The minimum residual always occurs at the center frequency s_0, where the residual is theoretically zero. As the difference between s and s_0 increases, the residual also increases.

While the Padé approximation was performed above with the s-parameters of the electromagnetic circuit, a similar procedure can be used with every element of the vector $x(s)$. This means the electromagnetic field behavior is also captured by using the AWE process. At first, this would seem to be a daunting task since the finite element solution vector is usually large. However, every element of the solution vector can be constrained to use the same poles, while the zeros can be obtained by simple summation. Thus, the expense of the calculation is minimized and we can readily plot electromagnetic field data versus position at any frequency. Indeed, the computer program HFSS allows users to plot electromagnetic fields at any frequency within the solution bandwidth from a single center frequency solution [12].

3. Adaptive Lanczos–Padé Sweep (ALPS)

To avoid the numerical instabilities in AWE, Feldmann and Freund have developed a procedure called Padé Via Lanczos or PVL [6]. PVL has the advantage of using the numerically robust Lanczos algorithm to compute the eigenvalues of the system, rather than the more problematic power method. It also has the benefit of providing error estimates of the resulting poles and zeros.

The relationship between AWE and the eigenvalues of the system is explained in [15]. Assuming that the frequency dependence of the system matrix $A(s)$ can be separated as $A(s) = A_0 + sA_1$ (where A_0 and A_1 are frequency independent matrices), we can rewrite (2) as

$$H(s) = (I - sM)^{-1} r(s) \tag{7}$$

where $M = -A_0^{-1}A_1$ and $r(s) = A_0^{-1}bu(s)$. Diagonalize the matrix M as

$$M = \chi \Lambda \chi^{-1} \tag{8}$$

where χ are the eigenvectors of M and $\Lambda = \mathrm{diag}(\lambda_1, \lambda_2, \ldots, \lambda_N)$ is the matrix of eigenvalues λ_i. Then (7) can be written as

$$H(s) = \chi(I - s\Lambda)^{-1}\chi^{-1}r(s) \tag{9}$$

This gives

$$H(s) = \sum_{i=1}^{N} \frac{\xi_i \cdot \rho_i}{1 - s\lambda_i} \tag{10}$$

where ξ_i and ρ_i are the ith row in χ and the ith column in $\chi^{-1}r(s)$, respectively.

Eq. (10) shows that the impulse response of a linear system can be treated as an eigenvalue problem and that the system poles are related to its eigenvalues. In theory, determining the system response requires that all of the eigenvalues of the matrix M be computed. However, in practice, it is sufficient to compute only the eigenvalues in or near the desired frequency range. This leads us to the Lanzcos algorithm. Consider the generalized eigenvalue problem

$$A_1\chi = -A_0\chi\Lambda \tag{11}$$

which has been derived from (8). The Lanczos algorithm approximates the eigenvalues of a large-dimensional matrix pair (A_0, A_1) with a sequence of small-dimensional matrix pairs (T_k, I), $k = 2, 3, \ldots, N$, where T_k is a tridiagonal matrix of dimension k. The eigenvectors of this ever growing sequence are in a vector space called a Krylov subspace. Details of this process are given in [16].

Although PVL is more stable than AWE, the Krylov vectors thus generated eventually lose orthogonality and the method stagnates. Sun has proposed a robust alternative to PVL based on Arnoldi iteration as modified by Parlett et al. [17,18]. In the original Arnoldi process, the newly-computed Krylov vector must be kept orthogonal to all previous Krylov vectors. This requirement is expensive and limits the method to small problems. However, Parlett and Scott showed that Krylov vectors lose their mutual orthogonality only when the Lanczos process converges to an eigenvector of the system [17]. By employing a measure to identify whether or not a Krylov vector has converged to an eigenvector; newly-computed Krylov vectors only need to be kept orthogonal to the set of converged eigenvectors. This is called selective orthogonalization and is much more efficient than the original approach. Compared to PVL, the new algorithm is not only numerically stable, but is also more efficient since it takes only one matrix–vector multiplication per Lanczos iteration and it simultaneously computes the multioutput parameters for a single input. Even when the computer runs out of storage for the Krylov and other vectors, one still obtains a spectral solution for a smaller frequency range. One can restart at another frequency to obtain the remaining spectral solution.

In the above, we assumed that quadratic and higher-order terms do not contribute to the Taylor series expansions (2). This is not entirely true, although these terms may be neglected if the frequency range is small enough. To obtain a wide-band response, we employ an adaptive process. Suppose that we are interested in the spectral domain response in the band $[f_{\min}, f_{\max}]$. We first compute two different reduced-order models using $f_{\min}$ and $f_{\max}$ as two different center frequencies. We then compute the spectral response of the system throughout the entire band $[f_{\min}, f_{\max}]$ using both reduced-order models. If the two responses are within an acceptable error tolerance throughout $[f_{\min}, f_{\max}]$, then the procedure has converged. However, if the two responses differ by more than the error tolerance, the frequency of maximum error $f_{\max}$ is noted. An additional reduced-order model is then computed using $f_{\max}$ as a new center frequency, and the error checking process is repeated in the two new subintervals. This process is repeated until the two reduced-order models bordering all subintervals give the same spectral response to within the set error tolerance. The several resulting reduced order models are then combined together in a piecewise fashion to form a single reduced-order model across the band of interest.

4. The transfinite element method

The time-dependent Maxwell's equations in stationary source free regions are

$$\nabla \times \vec{E} = -\mu \frac{\partial}{\partial t}\vec{H} \tag{12}$$

$$\nabla \times \vec{H} = \varepsilon \frac{\partial}{\partial t} \vec{E} + \sigma \vec{E} \tag{13}$$

where $\vec{E}$ and $\vec{H}$ are the time domain electric and magnetic fields, respectively and μ, ε and σ are the material permeability, permittivity, and conductivity, respectively. Eqs. (12) and (13) are solved directly in procedures such as the FDTD and TLM algorithms. Maxwell's equations in the s-domain are obtained by taking the Laplace transform of (12) and (13), assuming zero initial conditions, and rear-ranging terms

$$\nabla \times \vec{E} = -\mu(s - s_0)\vec{H} - \mu s_0 \vec{H} \tag{14}$$

$$\nabla \times \vec{H} = \varepsilon(s - s_0)\vec{E} + (\varepsilon s_0 + \sigma)\vec{E} \tag{15}$$

Here, $\vec{E}$ and $\vec{H}$ are the Laplace Transforms of $\vec{E}$ and $\vec{H}$, respectively, and s_0 is an arbitrary complex frequency. To increase computational efficiency, we eliminate either $\vec{E}$ or $\vec{H}$ by combining (14) and (15) to give a vector wave equation. In the following, we generate the vector wave equation in $\vec{E}$; a similar procedure can be used to generate an equation in $\vec{H}$. Taking the curl of (14) and using (15) gives

$$\nabla \times \frac{1}{\mu} \nabla \times \vec{E} + s_0^2 \left(\varepsilon + \frac{\sigma}{s_0} \right) \vec{E} = -\varepsilon(s - s_0)^2 \vec{E} - (s - s_0)(2\varepsilon s_0 + \sigma)\vec{E} \tag{16}$$

Setting $s_0 = j\omega_0$ and scaling both sides by μ_0 yields

$$\nabla \times \frac{1}{\mu_r} \nabla \times \vec{E} + k_0^2 \varepsilon_r' \vec{E} = -\frac{1}{\omega_0^2} [\varepsilon_r (s - j\omega_0)^2 + 2j\omega_0 \varepsilon_r''(s - j\omega_0)] k_0^2 \vec{E} \tag{17}$$

where $k_0 = \omega_0 \mu_0 \varepsilon_0$ is the wavenumber at frequency ω_0 and ε_r' and ε_r'' are the complex relative dielectric constants

$$\varepsilon_r' = \varepsilon_r - j \frac{\sigma}{\omega_0 \varepsilon_0} \tag{18}$$

$$\varepsilon_r'' = \varepsilon_r - j \frac{\sigma}{2\omega_0 \varepsilon_0} \tag{19}$$

Note that the electric field in (17) is a function of the complex frequency s relative to the center frequency ω_0.

The transfinite element method uses a combination of finite elements and mode matching to compute the electromagnetic field [19]. Consider an arbitrary N-port three-dimensional microwave device enclosing a domain Ω, bounded by perfect conducting walls $\delta\Omega$, and having N ports Γ_i, $i = 1, 2, \ldots, N$, illustrated in Fig. 1 with a 2-port.

In this case, the boundary conditions associated with (17) for an arbitrary–port structure are written as follows:

$$\hat{n} \times \vec{E} = 0 \quad \text{on } \partial\Omega \tag{20}$$

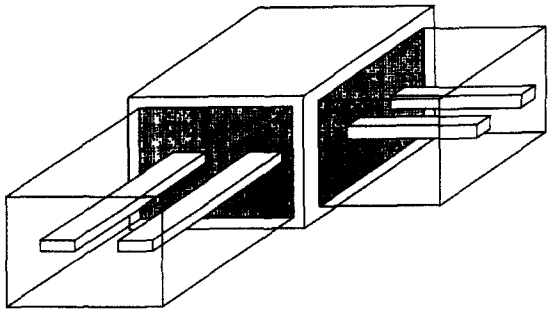

Fig. 1. Three-dimensional black box fed by two triaxial cables.

$$\vec{E} = \vec{E}^{\text{inc}} + \sum_{j=1}^{M_i} S^i j\vec{e}_j^{\,i} \quad \text{on } \Gamma_i \tag{21}$$

$$\vec{E} = \sum_{j=1}^{M_k} S^k j\vec{e}_j^{\,k} \quad \text{on } \Gamma, k = 1, 2, \ldots, N, k \neq i\,. \tag{22}$$

In (21) and (22), E^{inc} is the incident electric field and $\vec{e}_j^{\,k}$ is the electric field mode of the jth mode on the kth port. In the transfinite element method, the incident field is taken to be one of the eigenmodes and all eigenmodes are normalized to give unity Poynting vector

$$\oint_{\Gamma_i} (\vec{e}_j^{\,i} \times \vec{h}_j^{\,i}) \cdot \hat{n}_i \, d\Gamma = 1 \tag{23}$$

It can be shown that the coefficients S_j^k are the same as the elements of the N-port generalized scattering matrix [19]. The s-parameters computed in transfinite element method are variationally stationary and converge faster than the electric field. This allows them to be computed very accurately.

Following the procedures in [19–21], we expand the electric field as

$$\vec{E} = \sum_{j=1}^{N_e} E_j \vec{\gamma}_j \tag{24}$$

where $\vec{\gamma}_j$ are tangential vector finite elements. Applying Galerkin's method generates the s-domain transfinite element matrix equation

$$(A^{(1)} + \Psi)x(s) = \frac{j}{\omega_0}[(s - j\omega_0)^2 A^{(2)} + (s - j\omega_0)A^{(3)}]x(s) - b^{(1)} + \frac{j}{\omega_0}[(s - j\omega_0)^2 b^{(2)} + (s - j\omega_0)b^{(3)}] \tag{25}$$

Note that (25) provides the dependence on the complex frequency s explicitly. The matrices in (25) assume different forms depending on the number of ports. For simplicity, we present the expressions here for a 2-port. Let I stand for the interior unknowns, Γ_1 stand for the unknowns on port 1, Γ_2 stand for unknowns on port 2, P_1 and P_2 contain the tangential electric fields on port 1 and port 2, respectively, P_1^{T} stand for the transpose of P_1, ψ_1 and ψ_2 are the input power on ports 1 and 2, respectively, and $\{\vec{\gamma}_i,\ i = 1, 2, \ldots, N_e\}$ are a set of tangential vector finite elements, where N_e is the total number of vector basis functions used in approximating the electric field. In this case, the matrices in (25) may be written as

$$A^i = \begin{bmatrix} M_{II}^i & M_{I\Gamma_1}^i P_1 & M_{I\Gamma_2}^i P_2 \\ P_1^{\mathrm{T}} M_{\Gamma_1 I}^i & P_1^{\mathrm{T}} M_{\Gamma_1\Gamma_1}^i P_1 & P_1^{\mathrm{T}} M_{\Gamma_1\Gamma_2}^i P_2 \\ P_2^{\mathrm{T}} M_{\Gamma_2 I}^i & P_2^{\mathrm{T}} M_{\Gamma_2\Gamma_1}^i P_1 & P_2^{\mathrm{T}} M_{\Gamma_2\Gamma_2}^i P_2 \end{bmatrix} \tag{26}$$

$$\Psi = \begin{bmatrix} 0 & 0 & 0 \\ 0 & \psi_1 & 0 \\ 0 & 0 & \psi_2 \end{bmatrix} \tag{27}$$

$$M_{ij}^1 = \left\langle \nabla \times \vec{\gamma}_i \middle| \frac{1}{\mu_r} \nabla \times \vec{\gamma}_j \right\rangle - \langle \vec{\gamma}_i \,|\, \vec{\gamma}_j \rangle \tag{28}$$

$$M_{ij}^2 = -2k_0^2 \frac{\langle \vec{\gamma}_i \,|\, \varepsilon_r' \vec{\gamma}_j \rangle}{2j\omega_0} \tag{29}$$

$$M_{ij}^3 = -2k_0^2 \langle \vec{\gamma}_i \,|\, \varepsilon_r'' \vec{\gamma}_j \rangle \tag{30}$$

The solution vector $x(s)$ contains the electric field and the scattering parameters S_j^k. For a 2-port, it is

$$x(s)=\begin{bmatrix} E_I^1 & E_I^2 \\ s_{11} & s_{21} \\ s_{12} & s_{22} \end{bmatrix} \tag{31}$$

The right-hand sides $b^{(i)}$ in (25) all have the same structure. For a 2-port device, $b^{(i)}$ has two columns and is given by

$$b^{(i)}=\begin{bmatrix} b_1^i & b_2^i \end{bmatrix} \tag{32}$$

where

$$b_k^i=\begin{bmatrix} M_{I\Gamma_k}^i P_k \\ P_1^{\mathrm{T}} M_{\Gamma_k\Gamma_1}^i P_k - \gamma_{11}^i \\ P_2^{\mathrm{T}} M_{\Gamma_k\Gamma_2}^i P_k - \gamma_{22(11)}^i \end{bmatrix} \tag{33}$$

Here, the matrix γ is nonzero only in b^1.

The domain Ω of the structure may contain arbitrary conductors and materials. The tangential vector finite elements ensure the tangential continuity of the electric field and provide for the continuity conditions between materials through the natural boundary conditions in the variational principle. Impedance boundary conditions may be set on lossy conductors, zero tangential electric field is set on perfect conductors, and absorbing boundary conditions are set on open, radiating boundaries.

5. The mixed-potential integral equation

The following development is similar to that presented in [8,26] so here we will be brief. To apply the s-domain method to integral equations, we write with the mixed-potential integral equation in terms of the unknown distribution of surface currents $\vec{J}(\vec{r})$.

$$s\hat{n}\times\vec{E}^{\mathrm{inc}}=-\hat{n}\times\left[s^2\int_{S'}\bar{G}_A(\vec{r},\vec{r}')\cdot\vec{J}(\vec{r}')\,\mathrm{d}a'+\nabla\int_{S'}G_\phi(\vec{r},\vec{r}')\nabla'\cdot\vec{J}(\vec{r}')\,\mathrm{d}a'\right] \tag{34}$$

Here, $\bar{G}_A$ represents the dyadic Green's function for the vector potential, G_ϕ represents the scalar Green's function, and $\hat{n}$ is the unit vector normal to the surface at the field observation point $\vec{r}$. We assume that the only objects in the problem are perfect electrical conductors, so that the sum of the incident and scattered electric fields is normal to the surface.

Now approximate $\vec{J}$ in (34) with RWG basis functions $\{\beta_j\}$ [28]

$$\vec{J}=\sum_{j=1}^{n}J_j\vec{\beta}_j \tag{35}$$

Applying Galerkin's method provides

$$[K(s)+s^2M(s)]J=sE \tag{36}$$

where

$$\begin{aligned} K_{ij}&=\int_S\int_{S'}(\nabla\cdot\vec{\beta}_i)G_\phi(\vec{r},\vec{r}')(\nabla'\cdot\vec{\beta}_j)\,\mathrm{d}a'\,\mathrm{d}a \\ M_{ij}&=\int_S\int_{S'}\vec{\beta}_i\cdot\bar{G}_A(\vec{r},\vec{r}')\cdot\vec{\beta}_j\,\mathrm{d}a'\,\mathrm{d}a \\ E_i&=\int_S\vec{\beta}_i\cdot(\hat{n}\times\vec{E}^{\mathrm{inc}})\,\mathrm{d}a \end{aligned} \tag{37}$$

Although the matrices K and M depend on frequency through the Green's functions, we assume for the moment that they do not. This allows us to make a change of variables: $b = sE$ and $u = s^2$ to express (36) as

$$(K + uM)J = b \tag{38}$$

The ALPS procedure described in Section 3 may then be applied to find a piecewise rational function approximation to the frequency response over the band of interest.

6. Implementation of reduced order models in circuit simulation

After applying AWE or PVL to a finite element or boundary element formulation of Maxwell's equations, we ultimately arrive at a set of reduced order models for the power scattering matrix S describing the port behavior of the electromagnetic device:

$$b = Sa$$

By applying standard circuit definitions that relate the incident and reflected port wave variables a and b to the port voltages and currents v and i, it is possible to rewrite the scattering relationship in terms of standard circuit quantities:

$$Y_{\text{ref}}v - i = S_I(Y_{\text{ref}}v + i) \tag{39}$$

We introduce $Y_{\text{ref}} = Z_{\text{ref}}^{-1}$, a diagonal matrix whose positive real entries are the reference admittances for each electromagnetic port, as well as the *current-scattering matrix* S_I defined by

$$S_I = Z_{\text{ref}}^{-1/2} S Z_{\text{ref}}^{1/2}$$

The advantage of (39) is that it lends itself to direct implementation in a circuit simulator. An equivalent circuit model for this relationship is shown in Fig. 2. The overall procedure for producing the equivalent circuit is now summarized:

(1) Run an electromagnetic analysis on the structure of interest, using fast-sweep methods to find the scattering parameter matrix S over a broad frequency band.
(2) Perform reduced-order modeling on the entries of the S matrix.
(3) Convert it into a current-scattering matrix S_I.
(4) Write out the reduced-order models as frequency-dependent controlled sources in the form of a circuit deck for SPICE [23].

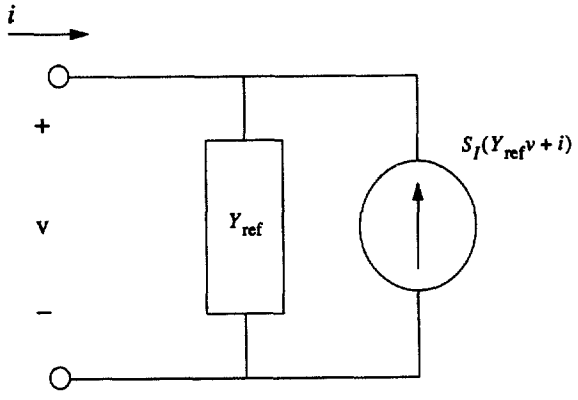

Fig. 2. A circuit interpretation of the current scattering relationship in (53).

7. Numerical results

Consider first the microstrip tee junction of [25]. The substrate is 0.0254 cm thick and has a relative dielectric constant of 9.9. The microstrip is 0.023 cm wide and is assumed to have zero thickness. The microstrip stub is 0.051 cm wide and 0.153 cm long. The geometry and computed numerical results are shown in Figs. 3 and 4. As Fig. 4 shows, the agreement between the present theory (solid lines) and the measured results (markers) obtained

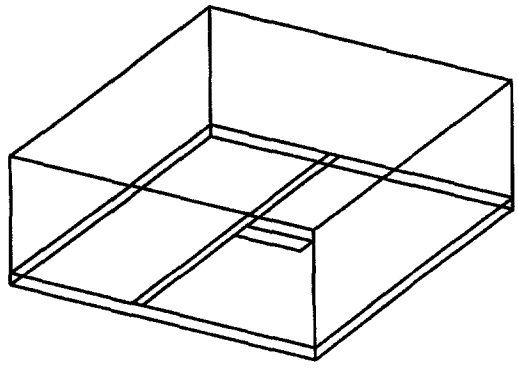

Fig. 3. A microstrip tee junction.

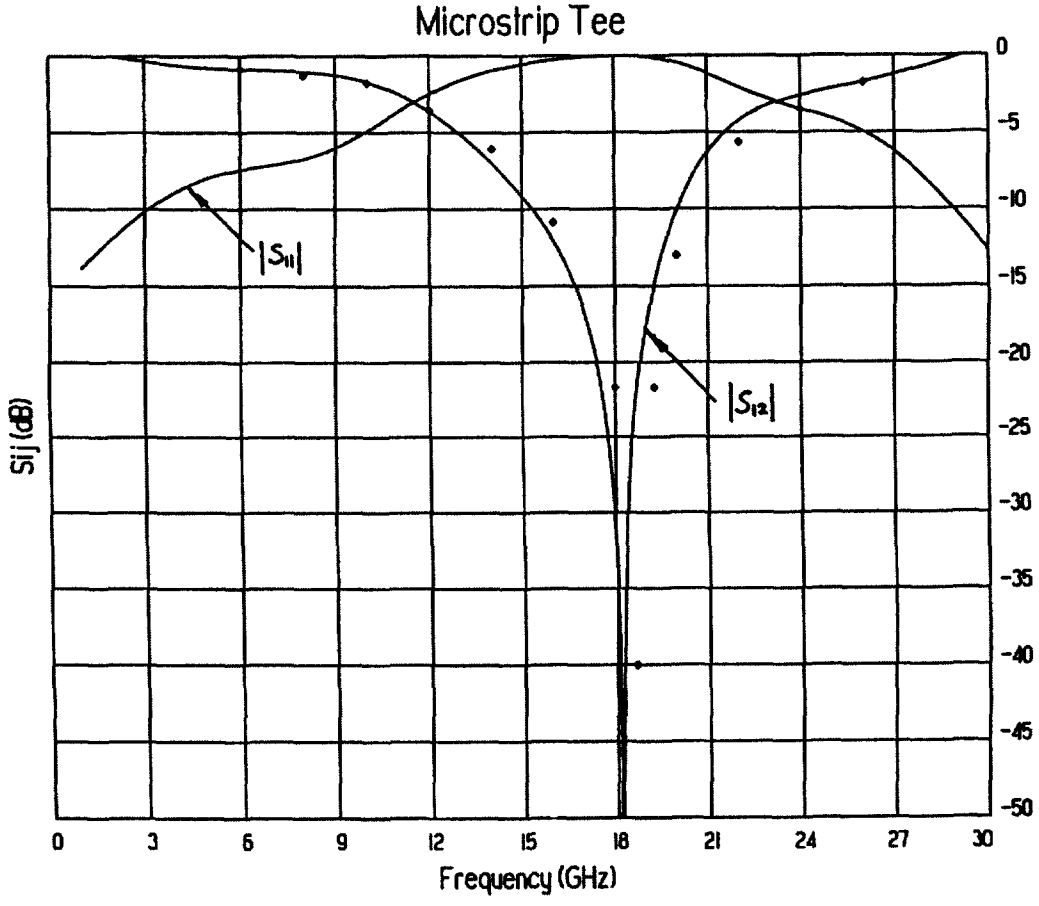

Fig. 4. Scattering parameters for the tee junction of Fig. 3. Solid line: calculated using AWE-based fast frequency sweep. Diamonds: measured results from [24].

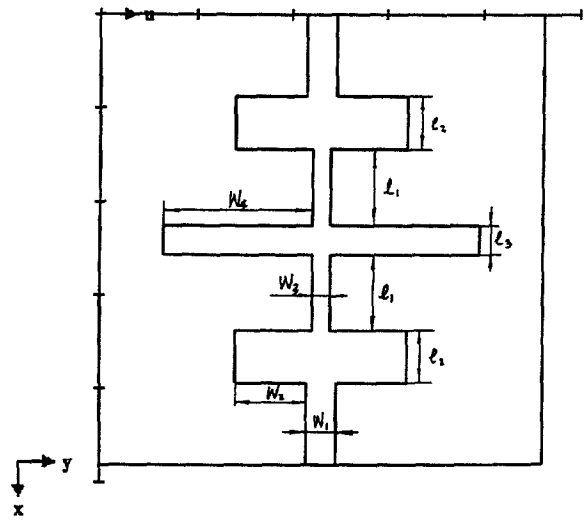

Fig. 5. A 3-pole microstrip filter design.

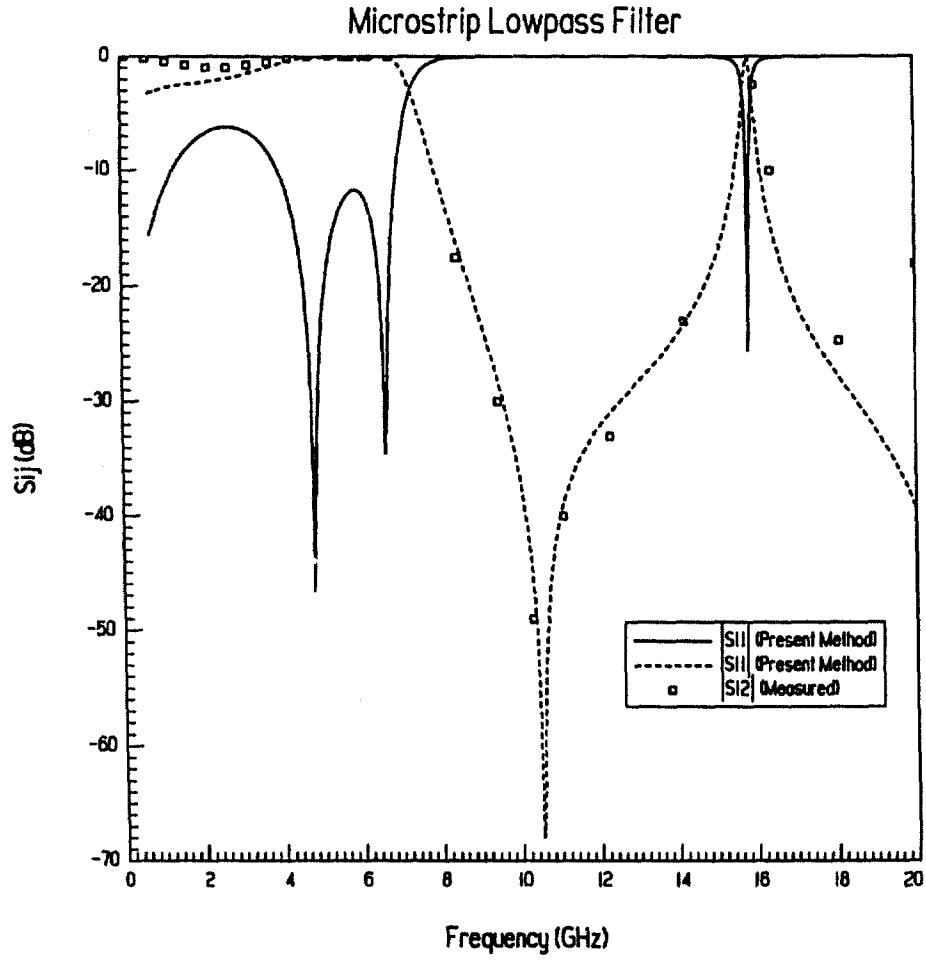

Fig. 6. Comparison of scattering parameters for the filter of Fig. 5. Solid lines: AWE sweep results; boxes: measured data.

by Giannini et. al. (Fig. 17(a) of [25]) is very good. The s-domain method performs a single matrix LU decomposition at 16 GHz and 16 additional forward and backward substitutions (i.e. 8 poles are used in the Padé approximation) and accurately predicts the spectral response over the 3 GHz to 30 GHz bandwidth. In contrast, with the frequency domain method, one would have to solve the matrix equation at many discrete frequencies to obtain a similar frequency response curve. Capturing the resonant frequency near 18 GHz is not trivial with the frequency domain method if one does not know the location of the resonance ahead of time. In contrast, this resonance is accurately and easily computed by the s-domain method.

To illustrate the efficiency of the s-domain method, consider the microstrip low pass filter shown in Fig. 5. The dimensions of the filter are: $l_1 = 65$ mil, $l_2 = 45$ mil, $l_3 = w_1 = 25$ mil, $w_2 = 60$ mil, $w_3 = 15$ mil and $w_4 = 125$ mil. The dielectric substrate has a relative dielectric constant of 9.6 and is 25 mil thick. Fig. 6 compares the present solution with measured results. Again, the agreement is excellent. Even though the spectral response of this filter is relatively complex, a single matrix solution at 12 GHz and 10 poles (20 additional forward/backward substitutions) are sufficient to obtain very accurate results over the wide band from 2 GHz to 20 GHz. The matrix size used in this example was 63214. The CPU time[1] required to perform a single LU decomposition was 107.5 min. However, it requires only 7.4 CPU minutes to perform a single forward/backward substitution. Thus, LU decomposition takes 14 times more CPU time than forward and backward

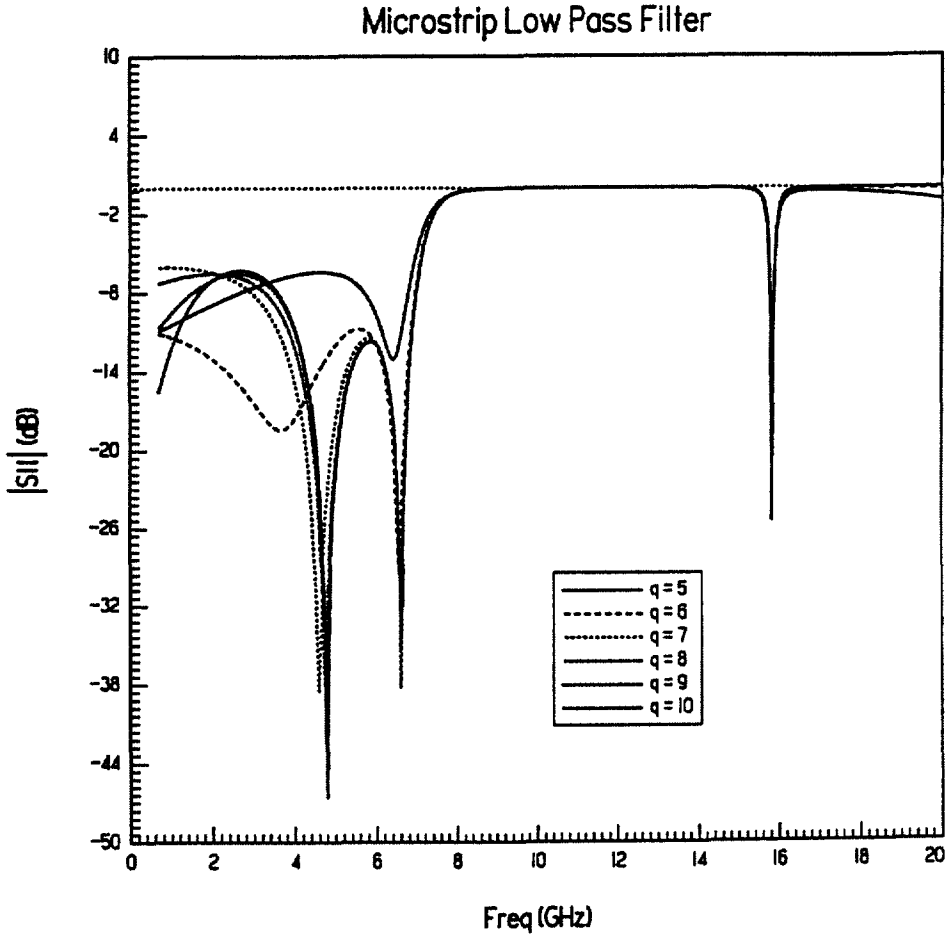

Fig. 7. Impact of the number of poles in the AWE approximation on the return loss for the filter of Fig. 5.

[1] These simulations were performed on an HP 9000/720 workstation with 64 MB RAM.

substitutions for this structure. Including the overhead of setting up this problem, the total CPU time for a single frequency point is $123.5 + 20 \times 7.4 = 271.5$ min. In contrast, if one were to solve the problem at 20 discrete frequencies, the total CPU time would be $20 \times 123.5 = 2470$ min. Thus, the s-domain method is approximately nine times faster and provides an analytic function for the spectral response versus the twenty discrete points obtained in the traditional method. With a spectral response as complicated as the one shown in Fig. 6, this analytical function is much more suitable for use in a microwave circuit simulation than are the twenty discrete values that must often be interpolated.

Figs. 7 and 8 illustrate the rate of convergence of the scattering parameters in terms of the number of poles used in the Padé approximation. The spectral response between 8 GHz and 18 GHz is correctly captured with as few as 5 poles. This indicates that the dominant poles that produces the peaks and valleys in the response are already contained in the five pole approximation. Additional poles improve the accuracy of the solutions at frequencies far away from the center frequency about the Taylor series expansion point.

As a third example, consider the rectangular waveguide discontinuity shown in Fig. 9. The waveguide is 19.05 mm wide and 9.524 mm high. The rectangular iris is centered with dimensions $w = 1.016$ mm, $l = 5.08$ mm and $h = 7.619$ mm. Fig. 10 compares the numerical scattering parameters with measured results obtained by

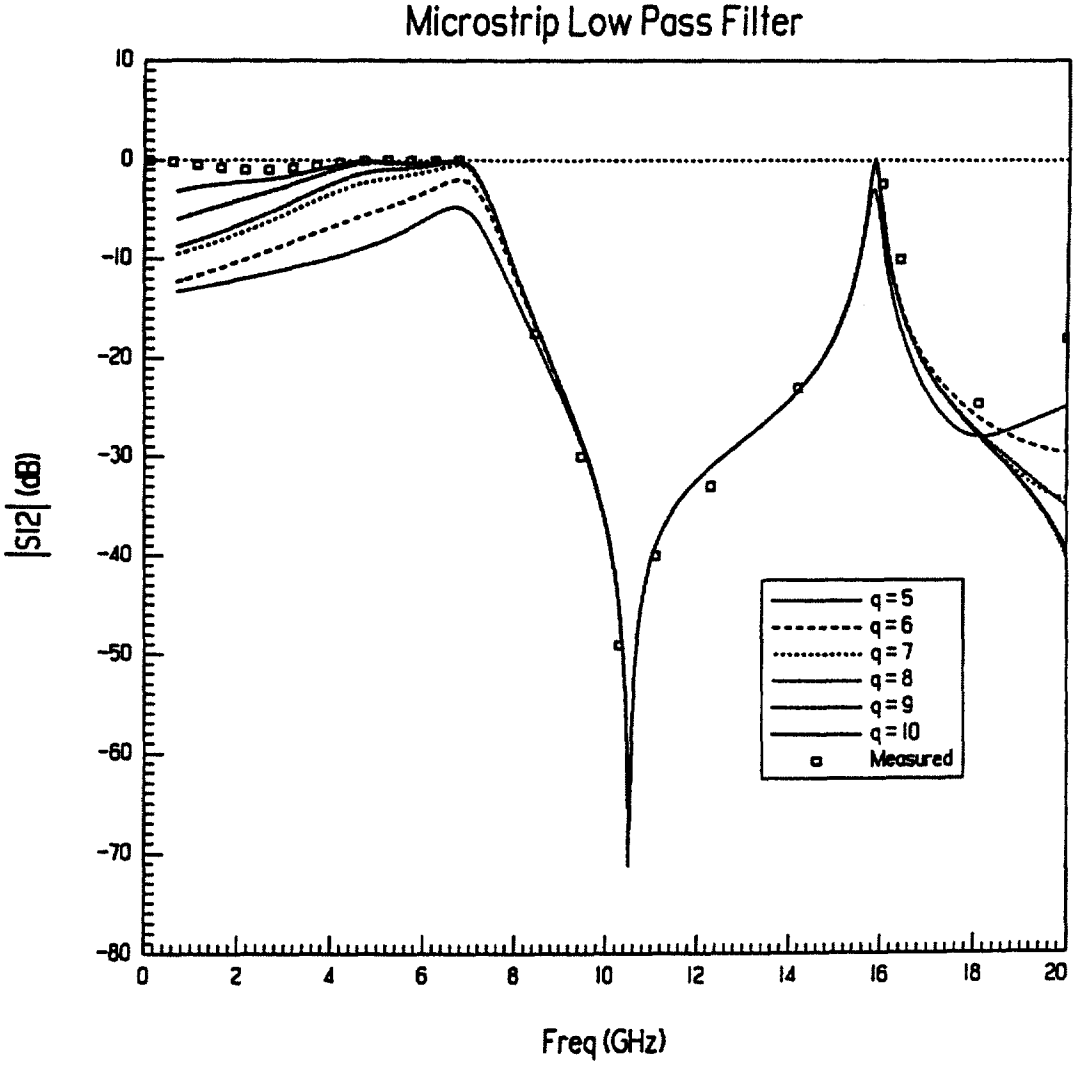

Fig. 8. Impact of the number of poles on the transmission coefficient for the filter of Fig. 5.

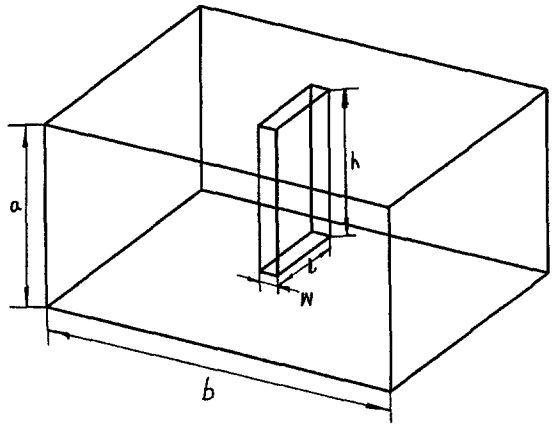

Fig. 9. A rectangular waveguide with a ridge discontinuity.

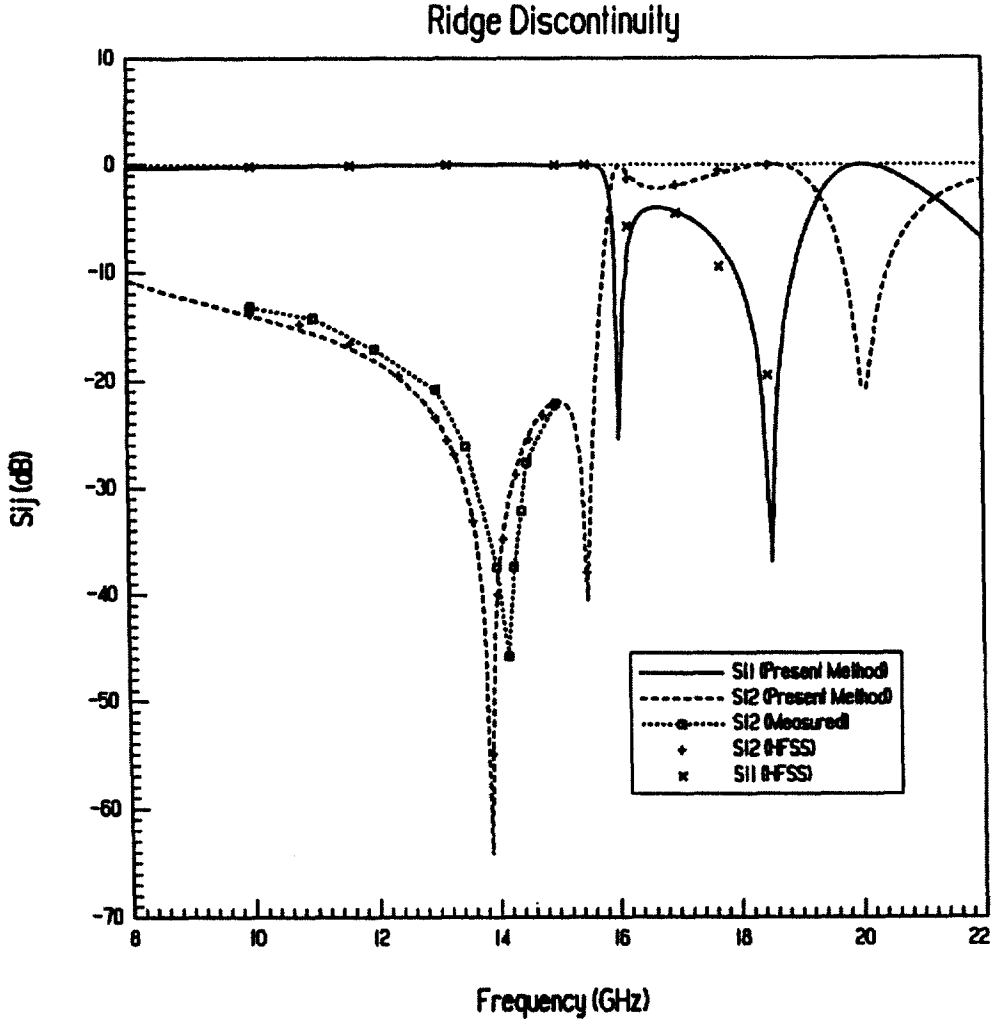

Fig. 10. The scattering parameters for the waveguide discontinuity of Fig. 9. The figure compares the AWE-based fast frequency sweep with measured data from [25].

Mansour et. al. (Fig. 6 of [26]). Figs. 11 and 12 again demonstrate the rate of convergence in terms of the number of poles used in the Padé approximations. With the center frequency at 13.0 GHz and 5 poles in the Padé approximation, the s-parameters are obtained accurately within the 10 to 15 GHz bandwidth. Adding poles to bring the reduced-order model up to 10 poles produces accurate solutions between 8 to 22 GHz. The latter set of results is confirmed by using the Ansoft High-Frequency Structure Simulator (HFSS) to perform a conventional 'discrete' frequency sweep.

The above three examples clearly demonstrate the power and the limitations of the s-domain method. It is evident that the solution is most accurate over a limited bandwidth. The range of this bandwidth depends on the number poles used in the model and on the complexity of the spectral response. Since the Padé approximation only catches dominant poles and zeros, the accuracy bandwidth decreases with increasing complexity in the spectral response. The global matrix residue error criterion in (6) indicates the range of validity of the Padé approximation. Fig. 14 presents the matrix residue plot for the rectangular waveguide cross-iris problem shown

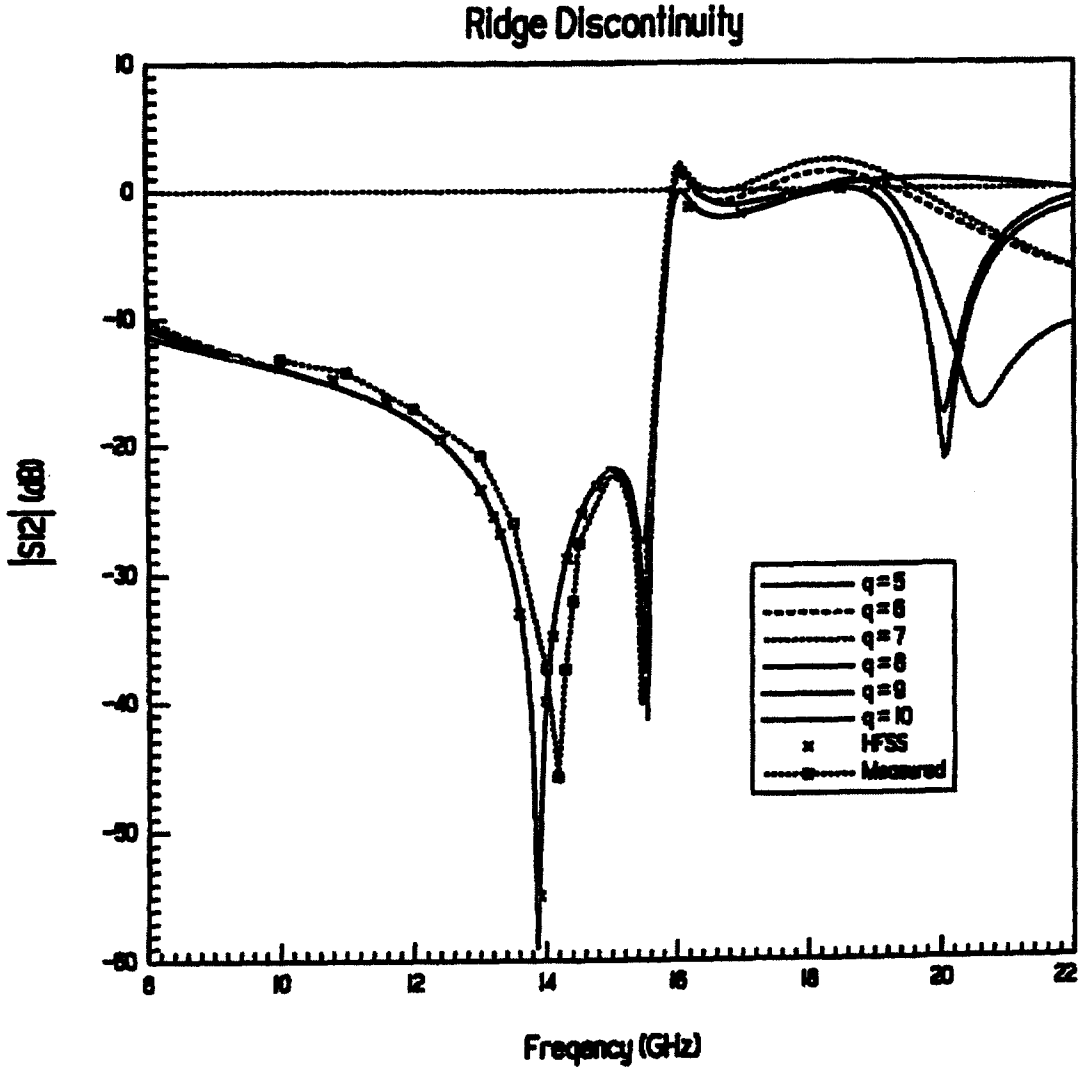

Fig. 11. Impact of the number of poles in the AWE approximation on the transmission coefficient for the waveguide of Fig. 9. Also shown (x) are the discrete frequency sweep results.

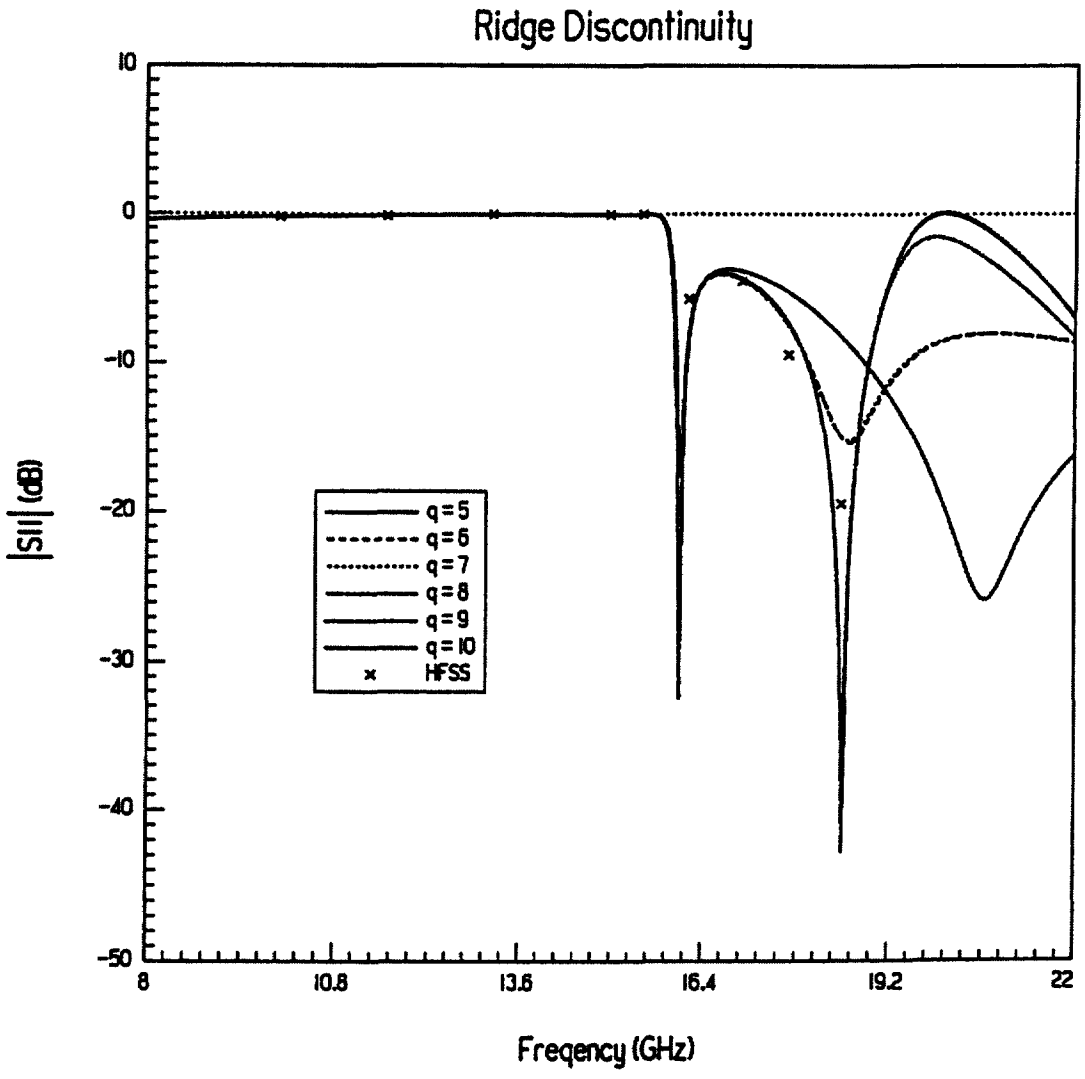

Fig. 12. Impact of the number of poles in the AWE approximation on the return loss for the waveguide of Fig. 9. Also shown (x) are the discrete frequency sweep results.

in Fig. 13. For this example, the minimum residue is located at the center frequency of 15 GHz where only round-off error occurs. Although the matrix residue is often less than 10^{-6} or -120 dB when it is directly decomposed, it is observed that the present method provides accurate scattering parameters for a large number of practical structure even when the matrix residue is as large as -20 dB. This is clearly illustrated in Fig. 14 where 10 poles are used in the Padé approximation.

The structure in Fig. 13 has a resonance around 15 GHz. To demonstrate the robustness of the method, the problem is solved at several center frequencies. Fig. 14 shows a typical matrix residue versus frequency plot for the case when the matrix is factored using 10 poles at the center frequency of 15 GHz. Fig. 15 shows that the center frequency has almost no effect on the spectral response even though the rational functions representing the system are different. This is an important property of the s-domain approach: one is not required to specify the solution frequency. Rather one must satisfy the loose requirement that the center frequency should be in the bandwidth of interest.

The next example demonstrates the use of fast sweep techniques for an integral equation solver. The problem is the low-pass filter structure shown in Fig. 16. This was analyzed using Strata, a full-wave boundary element

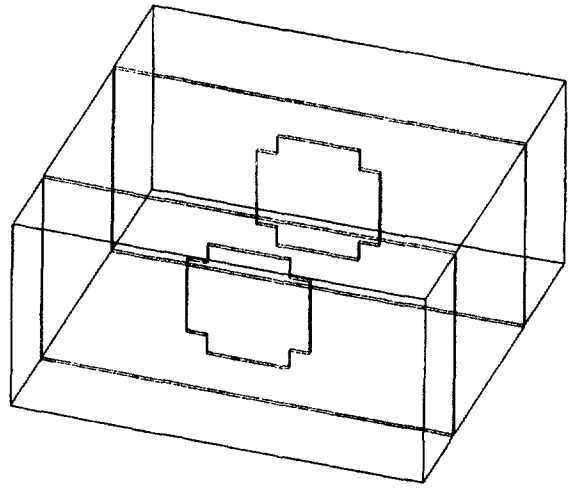

Fig. 13. A rectangular waveguide with two cross irises.

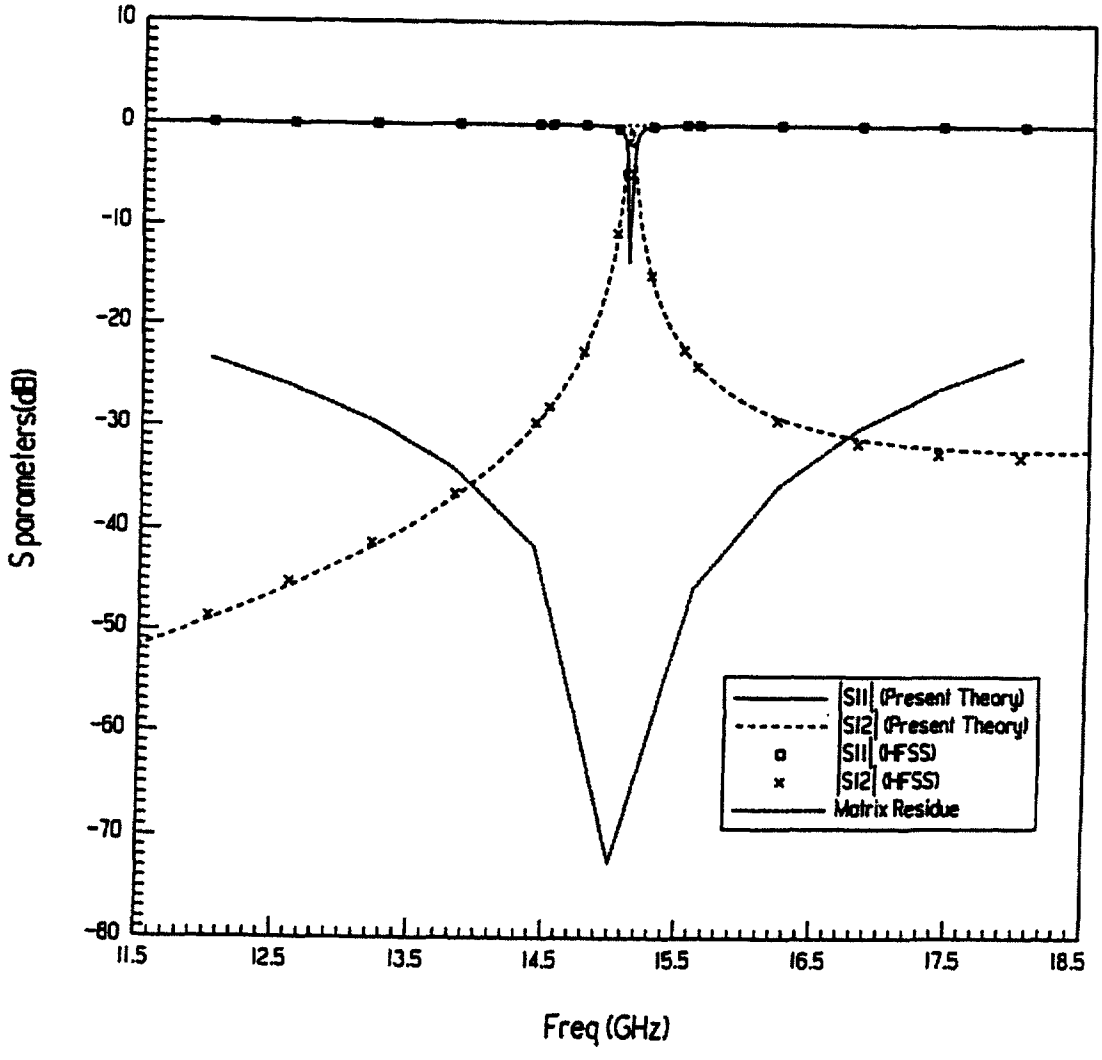

Fig. 14. Scattering parameters for the cross-iris problem of Fig. 13. AWE fast-sweep results are compared with HFSS discrete sweep results. Also shown is the matrix residual versus frequency.

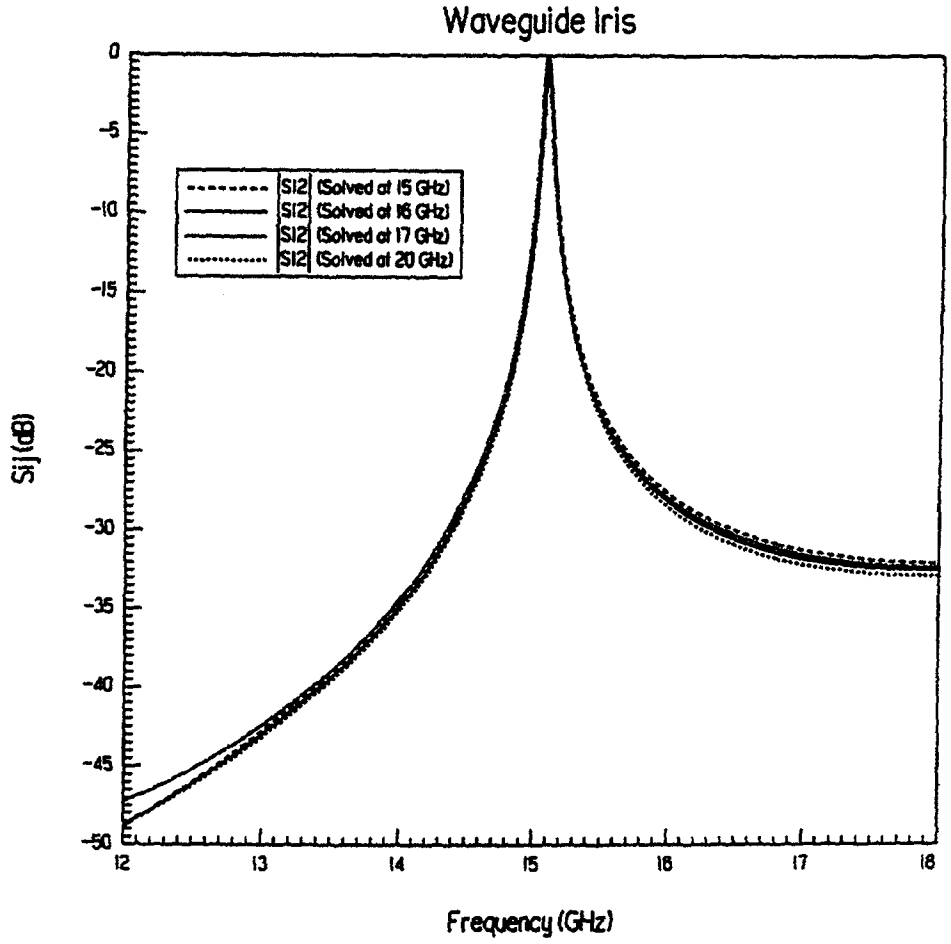

Fig. 15. Effect of the center frequency on the fast sweep approximation for the waveguide cross-iris problem of Fig. 13.

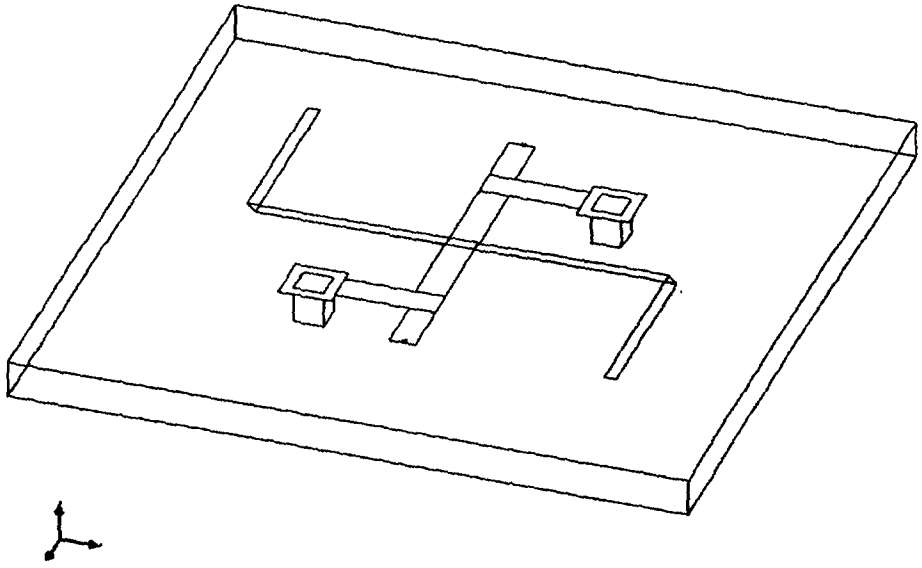

Fig. 16. A low-pass microstrip filter using grounded vias.

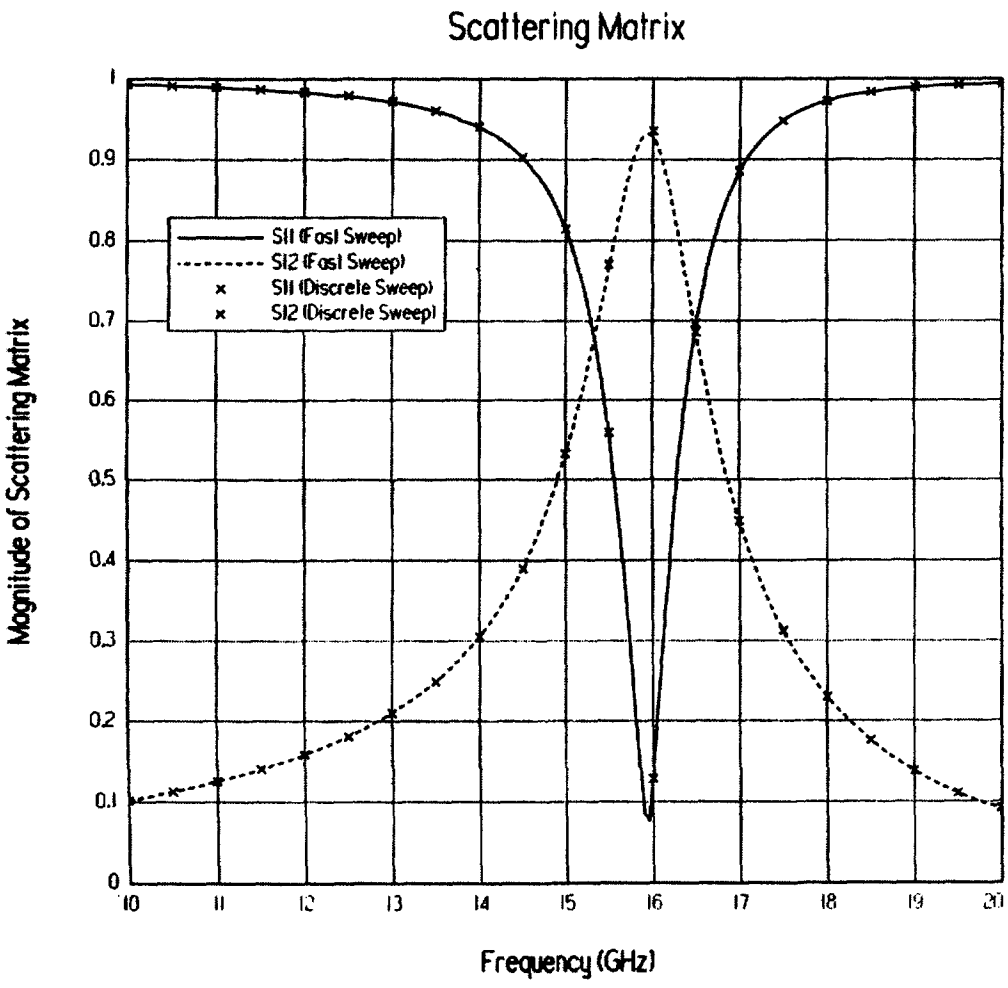

Fig. 17. Comparison of ALPS results with the conventional discrete frequency sweep in Strata.

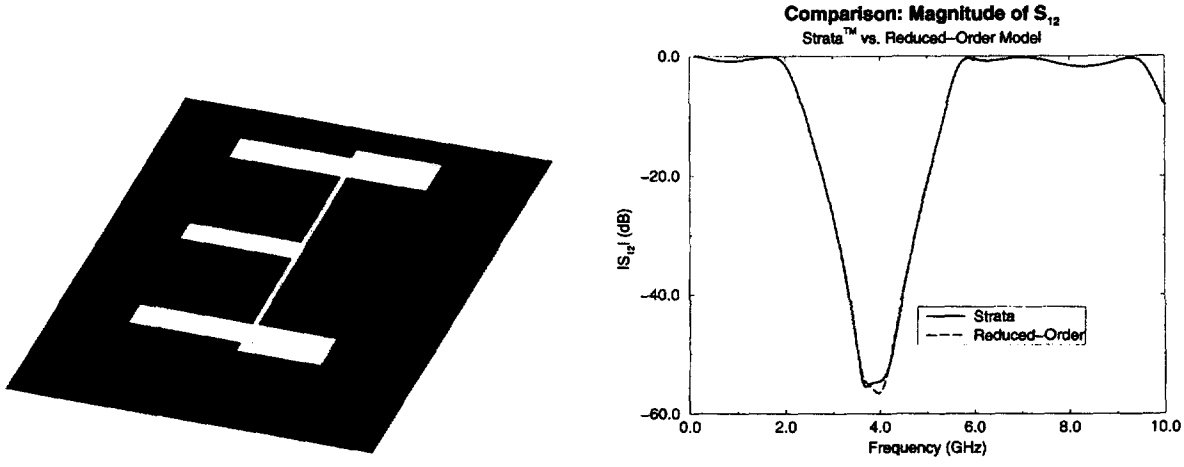

Fig. 18. Left: Chebyshev 3rd-order low-pass filter structure; right: comparison of Strata's frequency response (computed by fast sweep) and the reduced-order model.

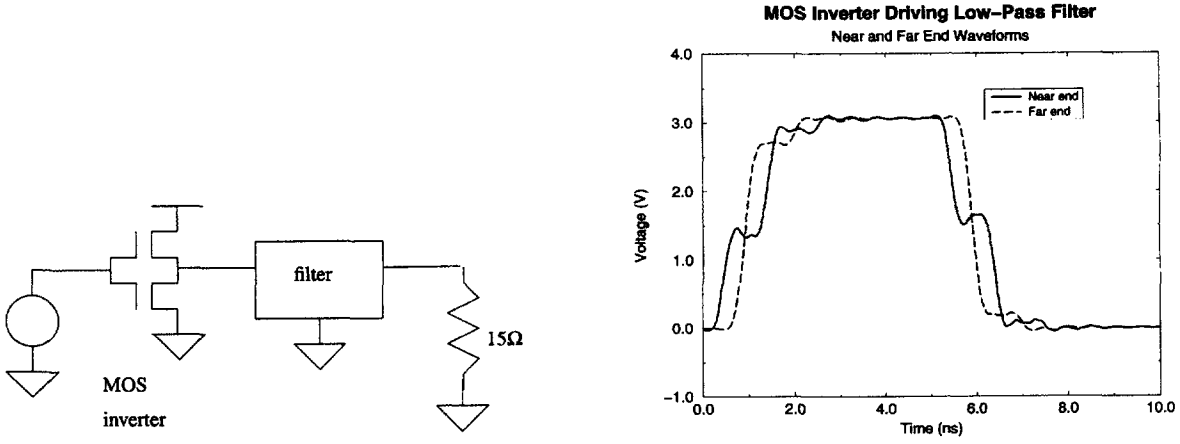

Fig. 19. Left: MOS driver combined with reduced order model; right: transient simulation results from HSPICE analysis.

code with ALPS-based fast frequency sweep. The results of the fast sweep are compared with a discrete frequency sweep (X's) in Fig. 17. The agreement is quite good across the entire frequency band.

Another low-pass filter is shown in Fig. 18 (left). The computed scattering parameters were modeled with rational functions of 16–18 poles. A comparison of the sweep results with the reduced-order model is shown in Fig. 18 (right).

A 2-port equivalent circuit model for the structure was then generated; this was connected to a nonlinear MOS inverter driver. The transmitted and reflected pulses from a transient simulation are shown in Fig. 19.

8. Conclusions

Fast frequency sweep methods provide a powerful tool for characterizing the electromagnetic behavior of structures that are intended to operate over a broad frequency band, or whose time-domain characteristics are important. Reduced-order models can be generated with a computational cost which is small compared to the field analysis at a single frequency. In this paper, we have demonstrated how fast sweep techniques may be applied to both finite element and integral equation formulations of the full-wave electromagnetic analysis problem.

For the finite element approach, the transfinite element formulation of Maxwell's equations was coupled with asymptotic waveform evaluation to compute the spectral response efficiently. Speed improvements of ten times or more over the traditional approach were obtained when analyzing typical microwave structures. In many cases, the spectral response over a wide bandwidth was accurately obtained by solving the problem at a single frequency and performing the AWE procedure. The solution is typically most accurate near the center frequency of the series expansion. However, it becomes less accurate as the frequency departs from the expansion point. The range of validity is problem dependent. If the frequency response of the structure is required over a broad band, additional solutions at different frequencies may be performed and then combined together using complex frequency hopping.

Alternatively, one may use the ALPS procedure, which adaptively solves at the frequency points of maximum error using the Lanczos algorithm with selective orthogonalization. The procedure is highly reliable and efficient. Typically, it needs fewer than 5 adaptive solutions. As shown in our test cases, excellent agreement is obtained between ALPS solutions and direct solutions. The ALPS procedure also makes it possible to apply fast sweep techniques to integral equation formulations of the electro-magnetics problem. For these formulations, the complicated frequency dependence of the matrices would prevent the use of the AWE or Lanczos procedures.

We have also explored the problems of efficient time-domain and mixed linear/nonlinear simulation. Reduced order circuit models were derived from the fast sweep results; these allowed us to characterize the time domain behavior of electromagnetic structures in the presence of nonlinear loading. Since the simulation of the nonlinear problem is carried out in a circuit-level tool such as SPICE, the analysis is orders of magnitude faster than can

be achieved in a field simulator. This permits the user to change the nonlinear device characteristics and resimulate without long delays.

References

[1] A. Taflove, Computational Electrodynamics: The Finite-Difference Time-Domain Method. (Artech House Boston, 1995).
[2] L.T. Pillage and R.A. Rohrer, Asymptotic waveform evaluation for timing analysis, IEEE Trans. on CAD, 9(4) (1990) 352–366.
[3] V. Raghavan, R.A. Rohrer, L.T. Pillage, J.Y. Lee, J.E. Bracken and M.M. Alaybeyi, AWE-Inspired, Proc. IEEE Custom IC Conf. (1993) 18.1.1-18.1.8.
[4] J.E. Bracken, V. Raghavan and R.A. Rohrer, Simulating distributed elements with asymptotic waveform evaluation, IEEE Intl. Microwave Symp. (1992) 1337–1340.
[5] E. Chiprout and M.S. Nakhla, Asymptotic Waveform Evaluation and Moment Matching for Interconnect Analysis (Kluwer, Boston, 1994).
[6] P. Feldmann and R.W. Freund, Efficient linear circuit analysis by Padé approximation via the Lanczos process, IEEE Trans. on CAD, 14(5) (1995) 639–649.
[7] E.H. Newman, Generation of wide-band data from the method of moments by interpolating the impedance matrix, IEEE Trans. Antennas Propagation, AP-30 (1988) 1820–1824.
[8] K. Kottapalli, T.K. Sarkar, Y. Hua, E.K. Miller and G.J. Burke, Accurate computation of wide-band response of electromagnetic systems utilizing narrow-band information, IEEE Trans. Microwave Theory Tech. MTT-39 (1991) 682–687.
[9] A.E. Ruehli, H. Heeb, J.E. Bracken and R. Rohrer, Three-dimensional circuit-oriented electromagnetic modeling for VLSI interconnects, Proc. IEEE Intl. Conf. Computer Design, Chicago, IL, 1992.
[10] X. Yuan and Z. Cendes, A fast method for computing the spectral response of microwave devices over a broad bandwidth, Proc. APS/URSI Intl. Symp., Ann Arbor, MI (1993) 196.
[11] D.-K. Sun, ALPS – an adaptive Lanczos–Padé approximation for the spectral solution of mixed-potential integral equations, USNC/URSI Radio Sci. Mtg. Digest, (1996) 30.
[12] HFSS User Manual, Hewlett-Packard Corporation and Ansoft Corporation, 1993.
[13] Maxwell Strata User Manual, Ansoft Corporation, 1996.
[14] G. A. Baker, Jr. Essentials of Padé Approximants (Academic Press, 1975).
[15] X. Huang, V. Raghavan and R. A. Rohrer, AWEsim: A program for the efficient analysis of linear(ized) circuits, IEEE Intl. Conf. on Computer-Aided Des. (1990) 534–537.
[16] C. Lanczos, An iteration method for the solution of the eigenvalue problem of linear differential and integral operators, J. Res. Nat. Bur. Standards 45 (1950) 255–282.
[17] B.N. Parlett and D.S. Scott, The Lanczos algorithm with selective orthogonalization, Math. Comput. 33(145) (1979) 217–238.
[18] B. Nour-Omid, B.N. Parlett and R.L. Taylor, Lanczos versus subspace iteration for solution of eigenvalue problems, Intl. J. Numer. Methods Engrg. 19 (1983) 859–871.
[19] Z.J. Cendes and J.-F. Lee, The transfinite element method for modeling MMIC devices, IEEE Trans. Microwave Theory Tech. 36(12) (1988) 1639–1649.
[20] J.-F. Lee, D.-K. Sun and Z.J. Cendes, Tangential vector finite elements for electromagnetic field computation, IEEE Trans. Magnetics 27(5) (1991) 4032–4035.
[21] Z.J. Cendes, Vector finite elements for electromagnetic field computation, IEEE Trans. Magnetics 27(5) (1991) 3958–3966.
[22] C. Hwang and Y.-C. Lee, Multifrequency Padé approximation via Jordan continued-fraction expansion, IEEE Trans. Autom. Control 34(4) (1989) 444–446.
[23] L.W. Nagel, SPICE2: A computer program to simulate semiconductor circuits, UC Berkeley Electronics Research Labs memo. no. UCB/ERL M520, May 1975.
[24] T. L. Quarles, Analysis of performance and convergence issues for circuit simulation, UC Berkeley Electronics Research Labs memo. no. UCB/ERL M89/42, April 1989.
[25] F. Giannini, G. Bartolucci and M. Ruggieri, Equivalent circuit models for computer aided design of microstrip rectangular structures, IEEE Trans. Microwave Theory Tech. 40(2) (1992) 378–388.
[26] R. Mansour, R.S.K. Tong and R.H. Macphie, Simplified description of the field distribution in finlines and ridge waveguides and its application to the analysis of E-plane discontinuities, IEEE Trans. Microwave Theory Tech. 36 (1988) 1825–1832.
[27] T. Sieverding and F. Arndt, Field theoretic CAD of open or aperture matched T-junction coupled rectangular waveguide structures, IEEE Trans. Microwave Theory Tech. 40(2) (1992) 353–362.
[28] S.M. Rao, D.R. Wilton and A.W. Glisson, Electromagnetic scattering by surfaces of arbitrary shape, IEEE Trans. Antennas and Propagation AP-30 (1982) 409–418.
[29] V. Raghavan, J.E. Bracken and R.A. Rohrer, AWESpice: A general tool for the accurate and efficient simulation of interconnect problems, in Proc. 29th IEEE/ACM Design Automation Conf. (1992) 87–92.